2004

Hindlimb function in the alligator: integrating movements, motor patterns, ground reaction forces and bone strain of terrestrial locomotion

Stephen M. Reilly

Jeffrey S. Wiley

Audrone R. Biknevicius

Richard W. Blob
Clemson University, rblob@clemson.edu

Follow this and additional works at: https://tigerprints.clemson.edu/bio_pubs

Hindlimb function in the alligator: integrating movements, motor patterns, ground reaction forces and bone strain of terrestrial locomotion

Stephen M. Reilly[1,*], Jeffrey S. Willey[1], Audrone R. Biknevicius[3] and Richard W. Blob[2]

[1]*Department of Biological Sciences, Ohio University, Athens, OH 45701, USA*, [2]*Department of Biological Sciences, Clemson University, Clemson, SC 29634, USA* and [3]*Department of Biomedical Sciences, Ohio University College of Osteopathic Medicine, Athens, OH 45701, USA*

*Author for correspondence (e-mail: reilly@ohiou.edu)

Summary

Alligator hindlimbs show high torsional loads during terrestrial locomotion, in sharp contrast to the bending or axial compressive loads that predominate in animals that use parasagittal limb movements. The present study integrates new data on hindlimb muscle function with previously obtained data on hindlimb kinematics, motor patterns, ground reaction forces and bone strain in order to (1) assess mechanisms underlying limb bone torsion during non-parasagittal locomotion in alligators and (2) improve understanding of hindlimb dynamics during terrestrial locomotion. Three dynamic stance phase periods were recognized: limb-loading, support-and-propulsion, and limb-unloading phases. Shear stresses due to torsion were maximized during the limb-loading phase, during which the ground reaction force (GRF) and caudofemoralis (CFL) muscles generated opposing moments about the femur. Hindlimb retraction during the subsequent stance-and-propulsion phase involves substantial medial rotation of the femur, powered largely by coordinated action of the GRF and CFL. Several muscles that actively shorten to flex and extend limb joints during stance phase in sprawling and erect quadrupeds act in isometric or even eccentric contraction in alligators, stabilizing the knee and ankle during the support-and-propulsion phase. Motor patterns in alligators reveal the presence of local and temporal segregation of muscle functions during locomotion with muscles that lie side by side dedicated to performing different functions and only one of 16 muscles showing clear bursts of activity during both stance and swing phases. Data from alligators add to other recent discoveries that homologous muscles across quadrupeds often do not move joints the same way as is commonly assumed. Although alligators are commonly considered models for early semi-erect tetrapod locomotion, many aspects of hindlimb kinematics, muscle activity patterns, and femoral loading patterns in alligators appear to be derived in alligators rather than reflecting an ancestral semi-erect condition.

Key words: locomotion, kinematics, kinetics, bone strain, motor patterns, alligator.

Introduction

Terrestrial tetrapods use diverse limb postures during locomotion, ranging from the highly sprawling posture of salamanders and some lizards (in which the limbs are held out to the side of the body; Ashley-Ross, 1994a,b; Reilly and DeLancey; 1997a,b; Rewcastle, 1981) to the parasagittal posture of birds and many mammals (in which the limbs are held more directly beneath the body; Jenkins, 1971; Reilly, 2000; Gatesy, 1990). Between these extremes, several species use intermediate postures (Jenkins, 1971; Gatesy, 1997; Pridmore, 1985), and some, such as crocodilians and some lizards (e.g. iguanas), are capable of using a range of limb postures even over a restricted range of speeds (Gatesy, 1991; Reilly and Elias, 1998; Blob and Biewener, 1999, 2001; Reilly and Blob, 2003). Studies of several different aspects of terrestrial locomotion in mammalian and avian species using parasagittal limb postures provided a foundation for discerning broad patterns in the mechanics and dynamics of tetrapod limb movements (e.g. Cavagna et al., 1977; Biewener 1989, 1990; Alexander and Jayes, 1983; Hildebrand, 1976; Demes et al., 1994; Blickhan and Full, 1992). However, an increasing number of studies on limb function in tetrapods using non-parasagittal limb postures have identified major differences in limb mechanics between animals that use parasagittal limb movements versus those that use non-parasagittal limb movements (Blob and Biewener, 1999, 2001; Reilly and Blob, 2003; Parchman et al., 2003; Willey et al., 2004). Among the foremost of these differences is the contrasting loading regimes found in the limb bones. Although there are some exceptions (e.g. the femora of chickens; Carrano, 1998), the limb bones of species using parasagittal limb movements are primarily loaded in bending or axial compression (Alexander, 1974; Rubin and Lanyon, 1982; Biewener et al., 1983, 1988). In

contrast, torsional loads exceed bending loads in species using non-parasagittal posture that have been examined to date (alligators and iguanas; Blob and Biewener, 1999, 2001).

Though torsional loads are clearly present in the limb bones of the non-parasagittal species that have been tested, the underlying causes of this torsion remain to be clarified. In the few vertebrates that have been found to exhibit strong torsional loading of limb bones (e.g. walking chickens, flying bats and birds; Pennycuick, 1967; Swartz et al., 1992; Biewener and Dial, 1995; Carrano, 1998), these torsional loads are believed to be induced by locomotor forces acting at a distance from the long axis of the limb bone which, therefore, generate a torsional moment. In species using non-parasagittal terrestrial locomotion, two different forces are likely to act at a distance from limb bone long axes and potentially contribute to torsional moments. First, because species using non-parasagittal locomotion hold their limbs out to the side of the body for much of limb support, the ground reaction force (GRF) will be directed either anterior or posterior to the long axis of limb bones for most of the step in these animals (Blob and Biewener, 1999, 2001). At the same time, the GRF will be directed more nearly perpendicular to the femur of non-parasagittal animals than it will be in parasagittal animals. As a result, the GRF will tend to rotate limb bones about their long axis in these species, contributing to torsional loading. Second, the major limb retractor muscle in many non-parasagittal species (including alligators and iguanas) is the caudofemoralis longus (CFL), which inserts on the ventral surface of the proximal femur (Snyder, 1962; Reilly, 1995; Gatesy, 1997). When this muscle contracts to retract the leg during the stance phase of locomotion, it acts at a distance from the long axis of the femur equal to the radius of the bone, and this distance is a moment arm for long axis rotation of the femur. Thus, contraction of CFL should produce inward (medial) rotation of the femur and torsional loading.

Though both mechanisms for the induction of torsion are viable, the relative contributions of each (and their potential interactions) are uncertain. As a result, it is difficult to predict whether torsion should be expected to predominate in the limb bones of all species that use non-parasagittal limb movements or whether specific differences in limb movements or mechanics might lead to alternative expectations for some lineages. To evaluate the contributions of these mechanisms to torsional loading of limb bones during locomotion, several types of data must be integrated, including information on limb position and movements, locomotor forces, muscular action and bone loading. The integration of such diverse sets of data is crucial not only for a complete understanding of bone loading mechanics, but also, ultimately, for a thorough understanding of the functional dynamics of how animals control forward propulsion with their limbs. Data on locomotor dynamics are available for only a narrow range of vertebrate taxa. Though studies focusing on multiple levels of analysis have provided major insights into propulsive dynamics in tetrapods, most studies have focused on animals with erect postures (cursorial mammals, primates) and, in particular,

bipedal species (kangaroos, birds, humans). To date, no study has combined analyses of locomotor forces, limb bone loads, motor patterns, kinematics and foot fall patterns to evaluate how a non-erect quadrupedal animal supports its body weight and generates propulsive forces with its limbs.

In this study, we present an integrative analysis of propulsive dynamics in the hindlimb of the American alligator (*Alligator mississippiensis* Daudin). By integrating data on limb forces, bone loads, kinematics and motor patterns, we are able to evaluate specific questions about locomotor mechanics in this species. In particular, we assess the potential mechanisms underlying limb bone torsion during non-parasagittal locomotion in alligators. Additionally, our analyses allow us to refine evaluations of limb muscle function and the roles that these muscles play in supporting body weight and retracting the limb. Based on limb movement, force and motor pattern data, we distinguish three dynamic phases during hindlimb stance: a limb-loading phase, a support-and-propulsive phase, and a limb-unloading phase. Comparisons of locomotor patterns among tetrapods suggest that limb function, forces, and the use of femoral rotation in alligators may be quite different from patterns understood for other species that use either more sprawling or more erect limb posture. These results suggest that species using non-parasagittal posture may exhibit considerable diversity in their locomotor mechanics. Furthermore, tail dragging has been shown to have serious consequences for locomotor mechanics in alligators (Willey et al., 2004) which are borne out in patterns of femoral function in this study. Thus, distinctive features of locomotor dynamics in alligators may be a consequence of dragging the tail rather than general features of non-parasagittal postures.

Materials and methods

This analysis re-examines and synthesizes data that were collected during the course of several studies of terrestrial locomotion in alligators, including studies of kinematics and gait (Reilly and Elias, 1998), *in vivo* limb bone strains (Blob and Biewener, 1999), locomotor forces (Blob and Biewener, 2001; Willey et al., 2004), and hindlimb muscle activity patterns (Gatesy, 1997; Reilly and Blob, 2003). Details of the methods used for data collection and initial analyses can be found in those publications. In the sections that follow, we summarize information on the methods used in these studies that are most relevant to our present analysis. Animals used in all of the studies on which our present analyses are based were provided by the Rockefeller Wildlife Refuge (Grand Chenier, LA, USA). All experimental procedures complied with IACUC guidelines for the institutions where data were collected.

In our synthesis of data from different sources, we based our analyses on trials that were collected from animals as similar in size as possible, under locomotor situations that were as similar as possible. In general, data were collected at temperatures between 22°C and 29°C, from subadult individuals 0.5–1.0 m in length and 0.5–4.0 kg in mass, at

speeds from 0.1–0.6 m s^{-1}, using a standard 'high walk' limb posture (limbs adducted 55±5° below horizontal at mid-stance), and a duty factor (ratio of hindlimb stance duration to stride duration) of approximately 0.7. Specifics for animal sizes, locomotor speeds and gait parameters are noted in the descriptions of methods provided for each set of experimental data. Although there is variation in some of these parameters, many were very closely matched across studies (e.g. mean duty factors across kinematic, force, bone strain and electromyography datasets ranged from 0.70–0.73). Moreover, we believe that over the extensive ranges of size and behavior of alligators, variation among the individuals and trials in our analyses is minimal, and that the insights gained from our synthesis outweigh the potential complications that arise from the combination of data collected during different experiments.

Kinematics and gait analyses

Kinematic angles and gait patterns were calculated and graphed to indicate the general position and direction of movement of the limb segments. Data on hindlimb kinematics and gait patterns were collected from five alligators (total length 0.48–0.54 m, body mass 247–333 g); detailed analyses for the strides used in the present analysis are presented in Reilly and Elias (1998). Alligators were filmed under strobe lights at 200 fields s^{-1} using a NAC HSV-400 high-speed video system. Both lateral and dorsal views of the alligators were filmed (using mirrors) as they 'high walked' on a 70 cm long canvas treadmill. Only strides during which the animals very nearly matched the speed of the treadmill (0.146 m s^{-1}) were analyzed, during which the position of a landmark painted on the hip stayed within a 1 cm zone (i.e. ±0.005 m). Based on the measured durations of these strides, the complete range of

speed variation among strides for all individuals was 0.141–0.151 m s^{-1}. This is less than 7% variation among strides, well within the range of variation reported in previous studies of alligator kinematics (Gatesy, 1991) and muscle activity patterns (Gatesy, 1997). Electromyographical data were collected from these exact same strides.

Reflective landmarks (2 mm diameter dots visible in both the lateral and dorsal views: Fig. 1A,B) were painted on the skin of the alligators to mark positions along the vertebral column (T), the hip joints (directly over the acetabula; H), and three landmarks on the right hindlimb: the knee joint (on the anterolateral point of the knee when flexed; K), the ankle joint (posterolateral point of the ankle when flexed; A) and the foot (lateral aspect of the metatarsal– tarsal articulation; F). Three-dimensional coordinates of each landmark were digitized using stereo measurement TV (sMTV; Updegraff, 1990), and kinematic angles were calculated from these coordinates with an accuracy of ±1° for each joint.

The knee and ankle angles calculated were the actual three-dimensional angles for these joints based on the landmarks above (Fig. 1B,C). Femoral movements were quantified using two three-dimensional angles: femoral retraction (retraction/protraction movements relative to the longitudinal axis of the pelvis) and femoral adduction (adduction/abduction position relative to the mediolateral axis of the pelvis). Femoral retraction was measured as the angle between the femur and a line from the acetabulum to the trunk landmark. This calculation produces angles that are 5–10° greater (not 15° as indicated by Reilly and Elias, 1998) than those that would be calculated if femoral position were measured relative to the sagittal plane (e.g. Gatesy, 1991) but produces kinematic profiles that are nearly identical (within 5–10%; Reilly and
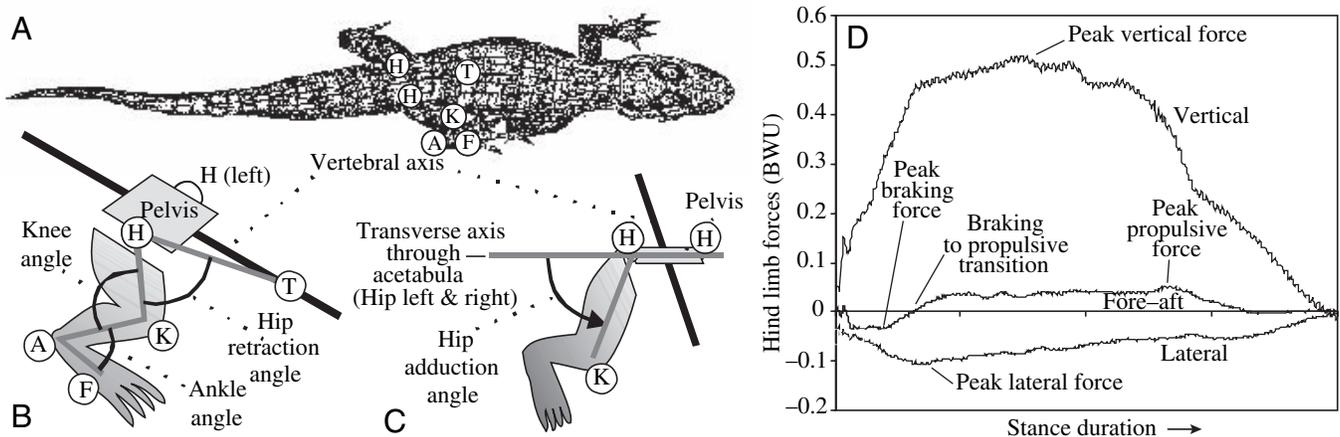

Fig. 1. Kinematic landmarks and angles used to describe hindlimb movements in alligators during locomotion. (A) Three-dimensional coordinates were digitized for one trunk landmark (T), and landmarks for the hip joint (H; on both sides: H left, H right); the knee (K), the ankle (A) and foot (F; on the skin on the lateral aspect of the metatarsal–tarsal articulation). (B) Three-dimensional angles were calculated for femoral retraction angle (the angle between landmarks T–H right-K indicating primarily femoral retraction/protraction movements); knee angle (angle H–K–A indicating knee flexion and extension), and ankle angle (angle K–A–F indicating foot flexion and extension). (C) Femoral adduction angle (angle H left-H right-K) was calculated to quantify the degree of hip adduction relative to a transverse line through the acetabula. (D) Ground reaction forces in body weight units (BWU) of a typical trial indicating key kinetic events: peak vertical force, peak braking force, braking-to-propulsive transition (zero fore–aft force), peak propulsive force and peak lateral force.

Elias, 1998). Femoral adduction was measured as the angle between the femur and a transverse axis through the acetabula (based on three-dimensional coordinates of both hips), with 0° indicating no femoral adduction (the femur held straight out laterally from the acetabulum) and 90° indicating a position parallel to the sagittal plane of the alligator (Reilly and Elias, 1998). This convention for reporting femoral adduction angles follows the evolutionary sprawling-to-erect paradigm, which categorizes sprawling femoral angles as 0° and erect ones as 90° (Bakker, 1971; Charig, 1972; Parrish, 1986, 1987; Reilly and Elias, 1998; Blob, 2001). Our femoral adduction calculations also account for pelvic roll about a longitudinal axis (<6° to each side; Gatesy, 1991) and, thus, effectively represent the angle between the femur and the horizontal plane of the body of the alligator. However, from a practical perspective, because pelvic roll is not very large in alligators (Gatesy, 1991) the difference between the convention of Reilly and Elias (1998) that we use in this analysis and conventions that refer to absolute planes is minimal.

Gaits used by alligators were identified by limb phase (Hildebrand, 1976; Reilly and Biknevicius, 2003), the elapsed time between a hindlimb strike and the ipsilateral forelimb strike normalized to hindlimb stride duration. Gaits used during kinematic, electromyographic, force platform and bone strain experiments had nearly identical duty factors and limb phase relationships.

For the analyses performed in this study, mean kinematic profiles and gait patterns for three-dimensional joint movements during high walks were taken from figs 4 and 5 of Reilly and Elias (1998). These plots were aligned with data on limb forces, limb bone strains, and limb muscle activity in order to evaluate how limb forces and their bone loading consequences are produced.

Electromyography

To quantify patterns of activity (motor patterns) for alligator hindlimb muscles during the high walk, electromyographic (EMG) recordings were collected from 12 muscles (all on the right side of the body). A previous study (Reilly and Blob, 2003) examined EMG data from the same alligator experiments but sampled muscle activity patterns across a range of femoral angles from 19–55° and compared ~30° to ~50° patterns to test for statistical effects of posture on the modulation of the timing and amplitudes of motor patterns. The present study presents new EMG data for the alligators normal high walk posture (femurs adducted 55±5° below horizontal at mid-stance), from the exact same strides (10 each from five animals of total length 0.48–0.54 m, body mass 247–333 g; speed (0.141-0.151 m s^{-1}) of treadmill locomotion examined in the synchronized kinematic analyses described above (Reilly and Elias, 1998).

EMG recordings were made from bipolar stainless steel electrodes implanted into each muscle as in previous research (Reilly, 1995). All electrodes were implanted while the animals were under anesthesia induced by placing the animals in a closed container with 1 ml of halothane for 15 min. Bared metal tips of each bifiler insulated electrode were 0.5 mm long. Electrodes were implanted percutaneously through the skin directly into the belly of each target muscle. The bundle of electrodes was glued together and sutured to a scale on the midline dorsal to the pelvis. Animals completely recovered from anesthesia within 2 h and all synchronized EMG and kinematic data were recorded during the next 2 h. Animals were rested (about 15–30 min) between bouts of walking (45 s maximum). Immediately following each experiment, the test animal was sacrificed by overdose of anesthetic and preserved in 10% formalin. Electrode position was then confirmed by dissection, and EMG data were considered valid for analysis only for preparations in which the electrode lay completely within the muscle.

EMG signals were amplified 10 000 times using AM Systems model 1700 differential AC amplifiers with a bandpass of 100–3000 Hz (and a 60 Hz notch filter) and then recorded on a TEAC XR-5000 multichannel FM tape recorder along with a synchronization pulse simultaneously recorded on the video frames. The analog signals (EMG channels plus a synchronization pulse) for each stride were converted to a digital data file using custom software with a Keithley analog-to-digital converter and a microcomputer. The effective sample rate for each channel was 10 kHz at 12-bit resolution. A 10 kHz sample rate was used because previous work has shown that this rate allows the faithful reproduction of EMG spikes from vertebrate locomotor muscles (Jayne et al., 1990). Prior to the experiments, an extensive calibration of the system revealed no crosstalk downstream of the electrodes, and crosstalk has not been a problem in previous work using the same electrode materials, construction and placement protocols. EMG profiles were inspected for possible patterns revealing crosstalk, and none were found.

Ten electrodes were implanted during each EMG experiment and, of these, five to six usually supplied successful data recordings, providing data from between one and three individuals for each target muscle (Table 1). Although we did not record from every target muscle in each of our five experimental alligators, we were able to record data from multiple individuals for seven muscles and it is upon these data that we based our primary conclusions. Custom software was used to digitize the times of burst onset and offset for each muscle relative to the timing of foot down within each stride. This was done to assess changes in muscle activity relative to the onset of stance phase (i.e. when the foot contacts the ground and limb movements begin to directly affect the propulsive dynamics of the limb cycle). To quantitatively characterize patterns of muscle activity, calculations of average burst patterns (EMG bars on Fig. 3F) were based on 10 strides from each individual for which muscles were successfully implanted. To facilitate the calculation of average EMG patterns among strides, and allow alignment of EMG, kinematic and gait data with force and strain datasets, durations of muscle bursts were scaled as a percentage of stride duration.

To gain more complete insight into muscular contributions to locomotor movements, forces and bone loading patterns

(including femoral torsion), we supplemented our own recordings of 12 muscle activity patterns with EMG data for four additional muscles published by Gatesy (1997). Details of the data collection methods for those muscles (caudofemoralis longus, flexor tibialis head 2, iliofibularis, and puboischiofemoralis externus head 2; indicated by asterisks in Table 1 and Figs 2, 3) are provided in Gatesy's original publication. Gatesy's data (Gatesy, 1997) can be reasonably compared to those for the other muscles examined in this analysis because Gatesy also collected EMGs during treadmill walking, and he recorded from animals of similar size (50–70 cm total length) under similar locomotor conditions (speed: 0.1–0.15 m s^{-1}; duty factor: 0.73±0.03; femoral adduction angle: 60°) to those used here. Gatesy's study (Gatesy, 1997) normalized burst timings to stride duration, but reported values relative to the onset of the caudofemoralis muscle burst. To coordinate data from Gatesy's study with EMGs from Reilly and Blob (2003) and force and strain records, Gatesy's burst timing data were adjusted by subtracting 6% from all onset and offset values (adjustment based on fig. 5 in Gatesy, 1997), thus realigning his EMG records relative to the beginning of stance phase. It should also be noted that eight muscles we recorded were also examined by Gatesy (1997). For two of these (flexor tibialis externus, iliotibialis head 2) our data provide positive verification of weak or sporadic patterns found by Gatesy (1997), and for the remaining six muscles EMG patterns were similar in both studies.

Myology

By combining EMG data from Gatesy (1997) with our EMG data, we were able to coordinate examination of the motor patterns of 16 alligator hindlimb muscles (including axial, thigh, and crural muscles) with kinematic, gait, force and bone strain data. Detailed anatomical descriptions of most of these muscles (except the tibialis anterior) have been published (Romer, 1923; Gatesy, 1997). However, to aid understanding of muscle function and our analyses, in this section we provide a brief summary of muscle morphology (together with a schematic illustration, Fig. 2). Previous studies have evaluated alligator muscle functions based on anatomical topography (Romer, 1923) or EMG patterns (Gatesy, 1997). By correlating EMGs with limb force and bone strain data, our present analyses allow us to test many of these proposed functions. Muscles are described in anatomical and functional groups based on results of Gatesy (1997), Reilly and Blob (2003), and this analysis. Refined details of muscle functions found in this study are presented in the results.

Posterodorsal thigh muscles (femoral retractors)

Flexor tibialis externus (FTE; Fig. 2A; one individual). Origin: tip of the postacetabular iliac process. Insertion: medially by a large tendon to the proximal tibia; distally by a smaller tendon passing down the leg to the calcaneus. It extends along the posterior aspect of the femur where it joins the heads of the flexor tibialis internus. FTE is the largest and
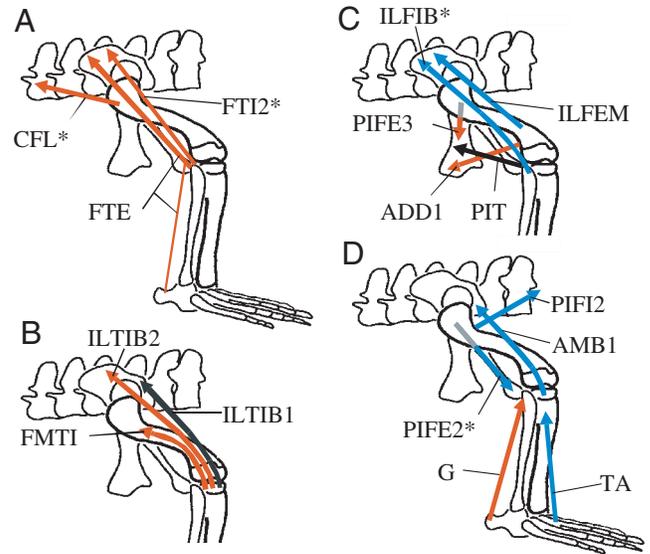

Fig. 2. Alligator hindlimb muscles involved in the high walking for which electromyographical data have been recorded. Lines of actions are indicated for muscles active in either stance phase (red), swing phase (blue) or with activity in both phases (black); gray shading in arrows indicates that the muscle lies medial to the femur. AMB1, ambiens, head 1; ADD1, adductor femoris 1; CFL, caudofemoralis longus; FMTI, femorotibialis internus; FTE, flexor tibialis externus; FTI2, flexor tibialis internus, head 2; G, gastrocnemius; ILFEM, iliofemoralis; ILFIB, iliofibularis; ILTIB1/2 iliotibialis, head 1/2; PIFE2/3, puboischiofemoralis externus, head 2/3; PIFI2, puboischiofemoralis internus, head 2; PIT, puboischiotibialis; TA, tibialis anterior. Data for muscles marked with asterisks are taken from Gatesy (1997). The continuation of the AMB1 tendon through the extensor sheet and into the Achilles tendon is not shown.

most posteriorly located muscle of the posterior thigh. FTE also functions as a knee flexor and ankle extensor (plantarflexor).

Flexor tibialis internus, head 2 (FTI2; Fig. 2A; two individuals). Origin: postacetabular iliac blade. Insertion: medially on proximal tibia. The FTI2 lies just ventral to FTE and is the largest of the four flexor tibialis internus slips. FTI2 shares a wide tendon with the puboischiotibialis (PIT) before inserting with the FTE on the proximal tibia. EMG data from Gatesy (1997).

Caudofemoralis longus (CFL; Fig. 2A; four individuals). Origin: caudal vertebrae 3–15, filling the space in the tail between vertebral haemal arches and transverse processes. Insertion: proximally by a tendon on to the fourth trochanter and surrounding area of femur; distally (not illustrated) by a smaller auxiliary tendon to the knee and calf musculature. The CFL is the largest muscle affecting hindlimb movements, producing femoral long axis rotation as well as retraction. EMG data from Gatesy (1997).

Anterodorsal thigh muscles (knee extensors)

Iliotibialis, head 1 (ILTIB1; Fig. 2B; one individual). Origin: anterodorsal rim of iliac blade. Insertion: *via* extensor

tendon over anterior surface of knee to the proximal tibia. The iliotibialis has three heads originating along the rim of the iliac blade. All three heads join the distal tendon of femorotibialis internus (FMTI) to form a common extensor tendon inserting on the front of the tibia. ILTIB1 is the most anterior of the three heads, smaller and deep to the ILTIB2.

Iliotibialis, head 2 (ILTIB2; Fig. 2B; two individuals). Origin: anterodorsal rim of iliac blade. Insertion: *via* extensor tendon over anterior surface of knee to the proximal tibia. The ILTIB2 is the middle head of the iliotibialis group. It is the largest muscle on the anterodorsal aspect of the thigh and originates from a wide portion of the iliac crest.

Both the ILTIB1 and 2 may play a role in hip and knee stabilization as well as knee extension (Reilly and Blob, 2003).

Femorotibialis internus (FMTI; Fig. 2B; three individuals). Origin: dorsal surface of central femoral shaft. Insertion: *via* extensor tendon over anterior surface of knee to the proximal tibia. The FMTI is the larger, more anterior belly of the two heads of the femorotibialis group. It shares a broad, tendinous insertion with femorotibialis externus, iliotibialis and ambiens.

Ventral thigh muscles (femoral adductors)

Adductor femoris 1 (ADD1; Fig. 2C; three individuals). Origin: ventral aspect of ischium. Insertion: ventral shaft of femur. The ADD1 is one of two heads of the adductor femoris muscle and the most superficial ventral muscle of the thigh.

Puboischiotibialis (PIT; Fig. 2C; 1 individual). Origin: anterior edge of ischium, well below acetabulum. Insertion: medial aspect of tibia. The PIT is a large muscle lying just posterior to ADD1. It passes along the ventral surface of the thigh to join FTI2 before inserting on the tibia.

Puboischiofemoralis externus, head 3 (PIFE3; Fig. 2C; two individuals). Origin: ventral surface of ischium. Insertion: Posteroventral surface of proximal femur. The three heads of the puboischiofemoralis externus complex converge to a common insertion on the proximal femur but are distinguished by their origins. The first and second heads (PIFE1 and 2) are more anterior and originate from the pubis and ribs, whereas PIFE3 is located more posteriorly.

Dorsal thigh muscles (femoral abductors)

Iliofibularis (ILFIB; Fig. 2C; three individuals). Origin: central iliac blade. Insertion: Fibular tubercle and gastrocnemius. The ILFIB extends across the hip and knee joints parallel to the femur. EMG data from Gatesy (1997).

Iliofemoralis (ILFEM; Fig. 2C; one individual). Origin: postacetabular iliac blade. Insertion: posterodorsal aspect of proximal femur. The ILFEM runs parallel to insert between the origins of the two heads of the femorotibialis group.

Anterior thigh muscles (femoral protractors)

Puboischiofemoralis internus, head 2 (PIFI2; Fig. 2D; one individual). Origin: centra of lumbar vertebrae and the ventral surfaces of their transverse processes. Insertion: Anterodorsal aspect of proximal femur. One of two heads in the puboischiofemoralis internus group, PIFI2 lies along the anterior surface of the proximal thigh. It is larger and originates more anteriorly than PIFI1 (not sampled).

Ambiens, head 1 (AMB1; Fig. 2D; two individuals). Origin: ilioischiadic junction anterior to the acetabulum. Insertion: proximally, over the anterior surface of the knee to the proximal tibia *via* the common extensor tendon with femorotibialis and iliotibialis; distally, a weaker tendon continues through the extensor sheet lateral the knee joint, inserting on the gastrocnemius and Achilles tendon (not shown). The AMB1 is a large muscle that extends along the anterior aspect of the thigh. AMB1 is one of two heads of ambiens that is more superficial and considerably larger than AMB2 (not sampled).

Puboischiofemoralis externus, head 2 (PIFE2; Fig. 2D; two individuals). Origin: ventral surface of the pubis and last abdominal rib. Insertion: posteroventral surface of the proximal femur. The PIFE2 runs from the anterior to the posteroventral aspect of the thigh. It is one of three heads of the PIFE group originating from the ventral pelvic elements that converge to insert on proximal femur. It is located anteriorly to PIFE3 (described above under femoral adductors). EMG data from Gatesy (1997).

Crural muscles

Gastrocnemius (G; Fig. 2D; three individuals). Origin: ventral aspect of distal femur and posterior proximal tibia. Insertion: calcaneal tuber *via* Achilles tendon. This ankle extensor is the largest muscle of the crus and appears to act as a knee stabilizer or flexor as well as ankle extensor (Blob and Biewener, 2001; Reilly and Blob, 2003).

Tibialis anterior (TA; Fig. 2D; two individuals). Origin: Anterior aspect of distal femur and proximal tibia and fibula. Insertion: Distal dorsolateral surfaces of the four most medial metatarsals. The TA passes through a laterally offset groove in the proximal end of the tibia to act as a dorsiflexor of the ankle.

Hindlimb ground reaction forces

To evaluate hindlimb ground reaction forces (GRFs) in the context of other datasets, a subset of GRF data reported by Willey et al. (2004) were selected that had been collected under locomotor conditions as close as possible to those of the kinematic, gait, and EMG data. GRFs were collected from five alligators (00.99–1.09 m total length; 2.24–4.00 kg body mass) as they walked over a force platform (Kistler Corporation, plate Type 9281B) inserted into a 6.1 m runway. To capture records for individual footfalls of the hindlimb and reduce the potential for interference from contacts with other feet, a triangular insert (244.25 cm) was firmly affixed to the surface of the force platform and made flush with the floor of the trackway, with the uninstrumented part of the track covering the rest of the platform. Analog signals from the force platform were amplified (Kistler Corporation, amplifier Type 9865C), digitized at 500 Hz, and imported into Bioware 2.0 software for analysis. Trials were synchronously recorded by two 60 Hz cameras (JVC TK-C1380U) oriented to provide views that would allow evaluation of whether footfalls were acceptable

for analysis (e.g. whether a single foot landed fully on the platform without overlapping feet). A single high-speed camera (Redlake Motionscope 500) simultaneously recorded the trials from a lateral view at 250 Hz in order to determine the velocity of each trial. Mean locomotor speed of each trial was determined from the time it took the animal to walk past a 70 cm calibration grid located on the back wall of the runway. Forward speeds were also calculated between successive 10 cm vertical bars immediately over the force platform. These velocities were compared with the mean velocity, and trials were accepted only if the successive velocities differed by less than 5% from the mean velocity (indicating the animals were not accelerating or decelerating). Duty factor (percentage of stride duration that the individual limb contacted the force platform) also was calculated from force and video records.

GRFs were collected in the vertical, fore–aft (craniocaudal), and mediolateral directions relative to the alligators (Fig. 1D). Vertical forces reflect body support and vertical acceleration of the center of mass due to gravity. Fore–aft forces are divided into braking (–) or propulsive (+) components. Mediolateral forces indicate whether a limb is pushing medially (+) or laterally (–). All GRFs were converted to body weight units (BWU) to adjust for differences in body mass among the animals. Five parameters of the GRF and their timing (percentage stance duration) were measured: peak vertical force, peak braking force, braking-to-propulsive transition (fore–aft force crosses zero), peak propulsive force, and peak lateral force.

From the 60 trials (12 runs per animal) analyzed by Willey et al. (2004), 20 high walk trials were selected from four of the alligators to produce a sample that very closely matched the mean speed ($0.146\ \mathrm{m\ s^{-1}}$) and duty factor ($0.70\pm0.01$) of the trials used in the analyses of kinematics, gait, and EMGs. This final sample (Table 2) included three to seven trials per individual, with a mean speed of $0.148\pm0.021\ \mathrm{m\ s^{-1}}$ and a mean duty factor of 0.70 ± 0.03. Gaits from steps used in the force measurements were found to be essentially identical to those used in the treadmill data collection. To compare patterns of GRF to other locomotor parameters, traces from typical GRF records were normalized to stance duration and aligned with kinematic, gait, and EMG data in Fig. 3 and with bone strain data in Fig. 4.

Femoral torsion

Profiles of locomotor forces, kinematics and EMGs were compared to evaluations of femoral torsion based on *in vivo* bone strain recordings (Blob and Biewener, 1999). Bone strains were recorded by surgically implanting strain gauges on the right femur of three subadult alligators (total length 0.98–1.04 m; body mass 1.73–2.27 kg) while the animals were under anesthesia (following protocols of Biewener, 1992). Rosette gauges were attached to the dorsal and ventral surfaces of the femur with cyanoacrylate adhesive, after the removal of a window of periosteum and cleaning of the attachment site with ether. Central elements of the rosette gauges were aligned with the long axis of the femur and indicated longitudinal

strains (tension or compression along the axis of the bone). The use of rosette gauges also allowed calculation of the magnitude and orientation of principal strains (maximum and minimum strains at a site, potentially not aligned with the long axis of the bone; Daley and Riley, 1978), as well as shear strains (calculated following methods of Biewener and Dial, 1995). These calculations allowed evaluation of the importance of torsional loading on the femur and the timing of its development through the stride cycle.

After gauge attachment, lead wires from the gauges were passed subcutaneously out of an incision dorsal to the acetabulum and soldered into a microconnector for connection to Vishay conditioning bridge amplifiers (model 2120, Measurements Group). After 2–4 days of recovery from surgery, data were collected during 40 s bouts of treadmill locomotion at either 0.17 or $0.37\ \mathrm{m\ s^{-1}}$ [note that Reilly and Elias (1998) found no speed effects on femoral retraction and adduction kinematics, thus we believe that strain data captured at slightly higher speeds should be comparable to the other data sets]. Raw strain signals were sampled through an A/D converter at 100 Hz and stored on computer for analysis. Locomotor trials were filmed with 60 Hz video to allow evaluation of limb movements, speed, and duty factor for each stride. To evaluate the timing of peak shear strains and the development of other strains relative to muscle activity and limb forces, representative strain traces were normalized for stride duration and aligned with traces for other locomotor parameters (see Fig. 4).

In addition to strain recordings, force platform records (Blob and Biewener, 2001) also provided data on femoral torsion by allowing calculation of the torsional moment of the GRF about the long axis of the femur. These data were obtained from six trials for a single alligator (1.98 kg) moving faster than those in the other datasets considered in this study ($0.62\pm0.21\ \mathrm{m\ s^{-1}}$) but using the same gait (fast walking trot; *sensu* Hildebrand, 1976). Data were collected from this alligator at 500 Hz as it walked down a runway and stepped with a single hind foot on a custom-built force platform (inserted so its surface was flush with the trackway) that measured the three-dimensional GRF. Using a mirror in the trackway, both lateral and dorsal views of the alligator were simultaneously filmed with a high speed video camera (250 Hz, Kodak EktaPro model 1012) as it stepped on the platform. The positions of the limb joints were digitized in the video frames and, combined with data on the magnitude and orientation of the GRF, the torsional moment of the GRF about the long axis of the femur was calculated using custom software. This moment indicates the tendency of the GRF to rotate the femur. If the GRF is directed posterior to the femoral long axis, it would tend to rotate the femur medially or inward (*counterclockwise* if viewing the right femur from its proximal end); if the GRF is directed anterior to the femoral long axis, it would tend to rotate the femur laterally or outward (*clockwise* if viewing the right femur from its proximal end). To evaluate the timing and direction of torsional moments relative to limb kinematics, muscle activity, and bone strains, a representative trace of the torsional moment

of the GRF was normalized for stride duration and aligned with traces for other locomotor parameters (Fig. 3B).

Results

Many features of the datasets we examined have been described in previous studies (Gatesy, 1997; Reilly and Elias, 1998; Blob and Biewener, 1999, 2001; Reilly and Blob, 2003; Willey et al., 2004). For this analysis, our results will focus on the three major areas: (1) description of motor patterns of four hindlimb muscles for which detailed descriptions have not previously been published, (2) coordinated analysis of kinematic, gait, and motor pattern data during the swing and stance phases of the locomotor cycle, and (3) the relative timing and coordination of landmark features of kinematic, gait, muscle activity, GRF, and bone loading data from the stance phase of the alligator hindlimb cycle.

Hindlimb muscle activity patterns

Mean motor patterns for 12 muscles quantified in this study and four from Gatesy (1997; indicated with asterisks) are presented in Table 1 and illustrated in Fig. 3F. For nearly all of the muscles that were examined by both Gatesy (1997) and here (Table 1), motor patterns were remarkably similar between the studies, with mean onsets and offsets differing by at most only 10% of stride duration. One exception was ILTIB2, for which we found burst durations to be longer by almost 20% stride duration (offsets of 52.3% *versus* 33.5% of stride duration). In addition, although some muscles recorded by Gatesy (1997) displayed pulsatile EMG signals, all of the muscles we recorded consistently showed discrete EMG bursts rather than pulsatile signals. For FTE and FTI2 in particular, we found discrete burst patterns that confirm the patterns identified by Gatesy (1997) from more sporadic bursts. Of the 16 muscles under consideration, eight had a majority of their activity during stance phase (red in Fig. 2), six were active primarily during swing phase (blue in Fig. 2), and two were active in both phases (black in Fig. 2), the continuously active ILTIB1 and the PIT with discrete bursts in both phases. Reilly and Blob (2003) provided the first summaries of motor patterns for four of these muscles (ILTIB1, PIFE3, G and TA) but their analysis focused on changes in burst characteristics related to limb posture, rather than propulsive dynamics. Therefore, we will describe the motor patterns of these four muscles in detail before outlining the new clarifications of muscle action patterns derived from coordinated analyses of the 16 muscles considered in this study. Summaries of mean onset and offset times for each muscle are reported in Table 1 and illustrated in Fig. 3F.

Iliotibialis, head 1

Extending from the dorsal pelvis to the knee (Fig. 2B), Iliotibialis, head 1 (ILTIB1) is in a position to abduct the femur and extend the knee. ILTIB1 has the earliest onset of any of the primarily stance phase muscles (Table 1), with activity beginning just before the middle of swing phase (–18% of

stride duration) and ending just after mid-stance (38% of stride duration). Its onset coincides with the beginning of both hip adduction and knee extension in mid-swing phase (Fig. 3E). Thus, ILTIB1 contraction seems likely to contribute to protracting the thigh and extending the knee during swing phase. However, ILTIB1 activity during stance phase coincides with a long period during which the knee and hip adduction angle are held nearly constant (Fig. 3E,F). Thus, ILTIB1 activity during stance phase appears to stabilize the hip and knee joints.

Puboischiofemoralis externus

This ventral thigh muscle extends from the ventral surface of the ischium to the proximal femur (Fig. 2C) and is in a position to adduct the femur. Puboischiofemoralis externus 3 (PIFE3) becomes active in the last quarter of swing phase and continues to fire for the first three-fourths of stance; thus, its activity coincides with the entire time during which the femur retracts. Because actual femoral adduction is slight during this period, PIFE3 appears to serve as hip stabilizer during stance.

Gastrocnemius

Extending from the posterior aspect of the knee to the heel (Fig. 2D) this muscle is clearly positioned to extend the ankle as well as flex the knee. It is active from just after foot down until almost the end (~90%) of stance phase. Ankle extension begins at about 35% of stance duration; thus, during the second two-thirds of its activity period, the gastrocnemius (G) clearly serves as an ankle extensor (plantarflexor). However, the ankle flexes during the first third of the activity period of the gastrocnemius. Contraction of the gastrocnemius during ankle flexion probably serves to control the degree of ankle flexion and, thereby, stabilize the ankle prior to the onset of its extension.

Tibialis anterior

Extending from the proximal tibia to the metatarsals (Fig. 2D) Tibialis anterior (TA) is well-situated to act as an ankle flexor (dorsiflexor). Corresponding to this role, TA is active in the first half of swing phase (68–91% of stride duration), essentially matching duration of ankle flexion during swing (Fig. 3). However, the TA was not active during ankle flexion in early stance phase suggesting that dorsiflexion at this time is a result of another muscle or passive effects of higher limb movements.

Motor control of swing phase hindlimb movements

Six muscles were active primarily during swing phase (Fig. 2C,D: blue). Although no ground reaction forces are associated with this portion of the limb cycle as the leg protracts, the motor patterns of muscles active during this time can be compared to joint kinematics to evaluate muscular function.

Femoral abduction and knee flexion

Of the many possible muscles in position to abduct the

Fig. 3. Integration of five levels of analysis of stance phase dynamics during hindlimb locomotion in alligators. (A) Dynamic phases of stance. (B) Torsional moment of the ground reaction force acting on the femur; illustrates torsional moments on the right femur as viewed from the acetabulum. (C) Three-dimensional ground reaction forces (top, vertical; middle, fore–aft; bottom, mediolateral) in body weight units (BWU). (D) Mean footfall patterns; R, right; L, left; H, hindlimb; F, forelimb. (E) Mean hindlimb kinematics. (F) Mean electromyographical patterns for 16 hindlimb muscles, constructed from the data in Table 1 and Gatesy (1997; indicated by *). All of the data (details in Materials and methods) are from alligators of similar size, moving at the same speed (~0.146 m s^{-1}), posture (femur adducted 51-60°), and gait (duty factors 0.70–0.73). Vertical green bars delineate the three dynamic phases of limb function (from A) during the stance phase: limb loading, support and propulsion and limb unloading, described in text.
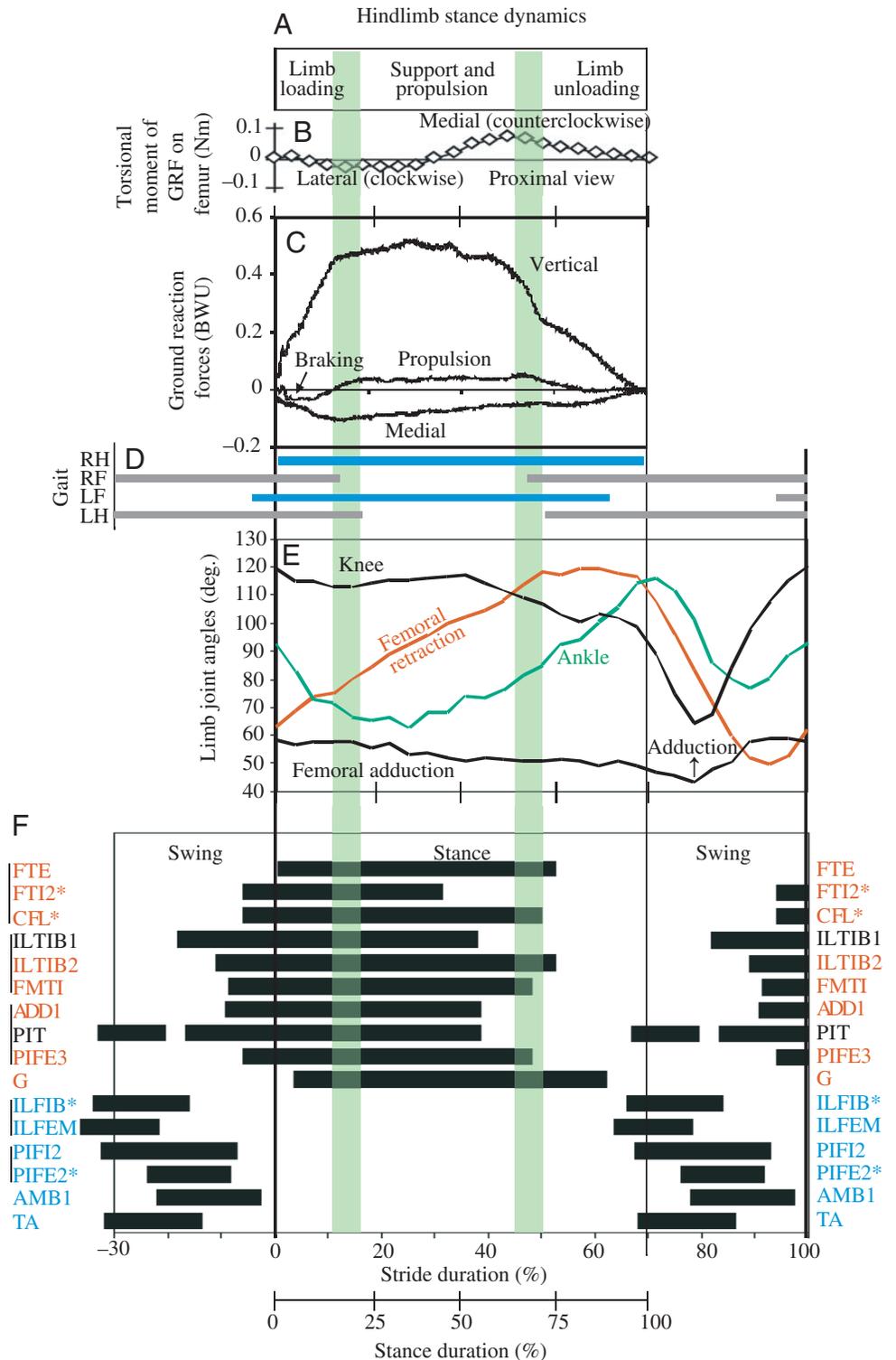
femur, only ILFIB and ILFEM (Fig. 2C) were active primarily during swing phase. Both muscles initiate their activity in late stance phase (Fig. 3F; first group of swing phase muscles). Activity in ILFEM, which is positioned to act solely as a femoral abductor, ends at about one third through the duration of swing phase, while activity in ILFIB, which passes over the knee joint, is active through nearly half of swing phase. These bursts coincide with the continuing abduction of the femur in early swing phase right after the foot is raised from the ground (Fig. 3E). These bursts also coincide with the swing phase burst of PIT, a femoral adductor. The synchronization of these bursts seems to indicate a controlled abduction (ILFEM) and adduction (PIT) of the femur early in swing phase before the femur is quickly adducted back to its position at foot down by the stance phase bursts of PIT and other femoral adductors. With regard to ILFIB, Gatesy (1997) showed that with its low origin on the iliac blade and oblique crossing of the knee joint, ILFIB is anatomically well positioned to flex the knee.

Correspondingly, the period of ILFIB activity matches the rapid period of knee flexion during early swing phase (Fig. 3E). Therefore, ILFIB appears to contribute to both femoral abduction and knee flexion in swing phase.

Femoral protraction and knee extension

Two anteriorly positioned, proximal thigh muscles, PIFI2 and PIFE2, exhibited focused bursts of activity in the swing

Table 1. *Patterns of hind limb muscle activity for alligators walking at 0.146 m s^{-1}*

Muscle	Abbreviation	Onset (%)	Offset (%)	N
Flexor tibialis externus	FTE	0.9±3.0	52.6±4.5	2
Flexor tibialis internus 2*	FTI2	–6.0±4.6	37.3±12.0	2*
Caudofemoralis longus*	CFL	–6.0±0.0	55.9±0.0	4*
Iliotibialis 1	ILTIB1	–18.0±6.5	38.0±7.3	2
Iliotibialis 2	ILTIB2	–10.9±7.2	52.3±5.3	2
Femorotibialis internus	FMTI	–8.4±1.9	48.2±3.2	3
Adductor femoris 1	ADD1	–9.4±4.1	38.7±5.5	3
Puboischiotibialis (stance burst)	PIT	–16.7±2.5	38.6±2.6	1
(swing burst)	PIT	67.2±3.9	79.5±2.4	1
Puboischiofemoralis externus 3	PIFE3	–6.0±2.7	48.1±4.1	2
Gastrocnemius	G	3.7±5.9	63.4±4.9	3
Iliofibularis*	ILFIB	66.1±5.5	84.0±3.0	3*
Iliofemoralis	ILFEM	63.6±2.3	78.3±1.4	1
Puboischiofemoralis internus 2	PIFI2	67.6±6.5	92.7±3.4	1
Puboischiofemoralis externus 2*	PIFE2	75.9±8.7	91.6±5.1	2*
Ambiens 1	AMB1	78.0±3.8	97.3±1.8	2
Tibialis anterior	TA	68.1±4.2	91.2±3.0	2

*Data for muscles studied by Gatesy (1997) moving at similar speeds (0.1–0.15 m s^{-1}) and posture (60° femoral adduction angle).

Mean timing variables (±S.D.) are measured relative to the time of foot down for each stride and scaled to stride duration. Ten strides per individual averaging 51° of femoral adduction angle at mid-stance and 70% duty factor are included for each individual (*N*) per muscle. These patterns are illustrated relative to other aspects of limb dynamics in Fig. 3F.

phase (Fig. 3F; second group of swing phase muscles). PIFI2 is positioned to oppose the action of CFL (Fig. 2D); thus, PIFI2 probably serves to protract the femur and rotate it laterally (in the opposite direction from CFL). Its activity closely parallels the period of femoral protraction during swing phase. PIFE2 is active in the latter half of femoral protraction during swing. Its ventral position (originating from the pubis) suggests it could contribute to femoral adduction during swing phase, but its anterior position suggests that, like PIFI2, PIFE2 may act as a primary protractor of the femur. The ambiens (AMB1, Fig. 2D) is also located in a position where its contraction could protract the femur. It is active somewhat later than PIFI2 and PIFE2, during the period of knee extension that occurs during femoral protraction (Fig. 3E,F). Because AMB1 spans the knee as well as the hip (Fig. 2D), the timing of its activity indicates it serves as a primary swing phase knee extensor as well as a limb protractor during late swing phase. Several other muscles that are anatomically positioned to extend the knee also become active during mid to late swing phase as knee extension commences. ILTIB1 activity begins just after that of AMB1 (Fig. 3F), indicating that ILTIB1 probably also contributes to the initiation of swing phase knee extension. ILTIB2 and FMTI become active toward the end of swing phase (Fig. 3F), so their contraction also may contribute to knee extension that occurs during this time (Fig. 3E).

Ankle flexion and extension

The ankle undergoes first flexion, then extension during swing phase. TA is anatomically situated to flex the ankle, extending from the tibia to the dorsal aspect of the foot (Fig. 2D). It exhibits a strong EMG burst during the first two-thirds of swing phase, coinciding very closely with the swing phase period of ankle flexion (Fig. 3E,F). Although G is anatomically located to act as a major ankle extensor, it is not active during swing phase ankle extension. However, AMB1 is active during mid to late swing phase, and its auxiliary tendon to the heel appears to have an important role in extending the ankle prior to the placement of the foot on the ground.

Motor control of stance phase hindlimb movements
Femoral retraction and rotation

Of the nine dorsally positioned thigh muscles considered in this analysis, only six were active during stance phase (Fig. 2A,B). Of these, three (FTE, FTI2, CFL; Fig. 2A, Fig. 3F; first set of three stance phase muscles) are positioned posteriorly and represent a functional unit that could retract and rotate the limb. CFL has been identified as the primary femoral retractor and medial rotator during limb retraction in crocodilians (Gatesy, 1990, 1997). EMG data show that CFL activity coincides with the entire period of femoral retraction, from its start during late swing phase until retraction stops nearly three quarters through the duration of stance phase (Fig. 3E,F). FTE and FTI2 are also located in positions suited to contribute to femoral retraction, and were considered ancillary stance phase hip retractors by Gatesy (1997). With insertions on the lateral aspect of the upper shank (Fig. 2A), both could also contribute to femoral rotation and, potentially, knee flexion (see below). However, these muscles have somewhat different motor patterns. FTI2 activity parallels the first two-thirds of the CFL burst, suggesting it contributes primarily to early retraction. Like CFL, FTI2 is situated to contribute to medial femoral rotation; however, FTI2 is active primarily when the GRF would tend to rotate the femur

laterally (i.e. in the opposite direction; Fig. 3B,F), suggesting that this muscle might help to stabilize the femur against rotation during early retraction. The same may be true for the CFL early in stance phase. In contrast, FTE has a later burst of activity, beginning at foot down and ceasing nearly simultaneously with the end of the CFL burst by the end of femoral retraction (Fig. 3E,F). The rotational moment of the GRF shifts from lateral to medial during this time, acting in the same direction as FTE and CFL by the midpoint of their bursts. This suggests that FTE, like CFL, contributes to femoral rotation as well as femoral retraction.

Knee stabilization and knee flexion

FTI2 and FTE are anatomically situated to flex the knee joint as well as retract the femur. However, during stance phase the knee joint is static before it flexes (Fig. 3E). Thus, FTI2, which is active only while the knee is static, appears to stabilize the knee rather than flex it. In contrast, FTE is active well into the period of knee flexion during the latter half of stance and, therefore, probably helps to actively flex the knee. Although knee flexion continues into late stance (Fig. 3E), activity ceases in both of these potential knee flexors well before the end of the step (Fig. 3F). Body weight might passively contribute to knee flexion during later portions of stance phase, but the hindlimb will tend to be unloaded when the next limb couplet of the trot contacts the ground later in stance phase (Fig. 3D; see later Results). As mentioned above, knee flexion during late stance might be actively controlled by the shank muscle gastrocnemius, which spans the flexor side of the knee joint and is active until almost the end of stance (Fig. 3F).

Three other dorsally positioned thigh muscles that are active during stance phase (FMTI, ILTIB1 and ILTIB2; Figs 2B, 3F; second set of three stance phase muscles) are aligned more closely with the long axis of the femur and share a wide tendinous insertion extending to the proximal tibia. These muscles all become active in mid to late swing phase as the knee extends (Fig. 3E). However, both the onset and offset of ILTIB1 activity are shifted earlier relative to those of the other two muscles by almost 20% stance duration. Unlike ILTIB1, both ILTIB2 and FMTI become active during the end of swing phase and fire through the first three quarters of stance phase. Gatesy (1997) reported knee extension during the latter half of stance phase and, therefore, described these three muscles as stance phase knee extensors. However, because our results (and data on other speeds and postures; Reilly and Elias, 1998) show the knee remaining static or flexing during stance phase, we conclude that these muscles act to stabilize the knee as it accommodates and supports body weight through the first three quarters of stance. In fact, it is not until activity ceases in these muscles that stance phase knee flexion becomes substantial, further suggesting that these muscles act to limit knee flexion during stance and that late in stance they no longer counter the effects of body weight and flexor muscles on the knee joint.

Femoral adduction

The last three thigh muscles active during stance phase (ADD1, PIT, PIFE3, Figs 2C, 3F; third set of three stance phase muscles) are anatomically situated to act as femoral adductors. These three muscles are active from mid to late swing phase until well into stance phase, but their burst patterns are somewhat staggered in time. PIT appears to act as a swing phase femoral adductor, becoming active before the middle of swing phase coincident with a major period of femoral adduction. There are two lines of evidence that the PIT actively powers adduction during the swing phase. First, the swing phase burst is associated with the complete repositioning of the limb in adduction during swing (Fig. 3E,F). Second, the swing phase PIT EMG intensity (mean area) is approximately the same as that during stance phase (Reilly and Blob, 2003). In contrast, ADD1 and PIFE3 become active in the last third to fourth of swing phase, after femoral adduction has stopped. All three muscles are active through most of the first three quarters of stance, but PIFE3 activity continues longer than that of the other muscles, lasting until femoral retraction stops and vertical GRFs begin to decrease. Because the activity of these muscles coincides with phases when the femur is static (or actually abducted as much as 5°), these three muscles appear to stabilize the hip, counteracting the weight of the body as it is supported during stance phase.

Ankle extension

The remaining stance phase muscle studied was the G, which appears to be a primary ankle extensor (Fig. 1D; Fig. 3F; last stance phase muscle). Our EMG data show that G activity begins after the start of stance and continues longer than that of any other stance phase muscle (until nearly 90% stance duration). Its activity begins near the end of ankle flexion during early stance and continues through the entire period of ankle extension during stance phase. It is not active during swing phase; thus, another muscle must control ankle extension that occurs while the foot is not in contact with the ground. It is noteworthy that FTE not only has an auxiliary tendon extending to the calcaneum, but that it has essentially the same motor pattern as G. Thus, FTE seems likely to also contribute to stance phase ankle extension.

Hindlimb ground reaction forces

Typical three-dimensional GRF traces for alligator hindlimb steps for animals moving the same speed as in the EMG studies are presented in Fig. 3C. Means for key events of the force patterns are presented in Table 2. Alligator hindlimb steps exhibited vertical force profiles that consistently increased to near peak values of about half of body weight in the first fifth of the stance phase. Near peak forces are maintained until about the last third of stance phase when body support wanes. Fore–aft forces indicate a brief braking component in the first fifth (15.4%) of stance phase with maximum braking force of 5.4% of body weight at 6% of stance duration. Thereafter, a long gradually increasing propulsive component occurs during the middle (from 15.4 to 64.4%) of stance phase coincident with the period when vertical forces plateau. Maximum propulsive force of 5.9% of body weight occurs at 64.4% of

stance duration. Propulsive effort then decreases to around zero early in the last third of stance duration. Mediolateral GRFs are consistently negative (i.e. medially directed), and these forces reach maximum values of about 10.6% of body weight in the first fifth (19.1%) of stance duration and then gradually decrease over the rest of the stance phase, dropping to zero just before the foot is picked up.

Hindlimb force vectors

Ground reaction forces were reconfigured to reflect hindlimb output forces. Sagittal (Fig. 4A) and transverse (Fig. 4B) two-dimensional limb force vectors illustrate how the hindlimb pushes on the ground during the stance phase. Once the foot has settled in after impact the net hindlimb vertical force vector is directed about 10° anterior to vertical (~80° on Fig. 4A) and about 60° lateral to the direction of travel (Fig. 4B). In the first one-fifth of stance phase the hindlimb force vector swings posteriorly to about 4° posterior to vertical (~94° in Fig. 4A) and 110° relative to the direction of travel. Throughout the middle portion of stance, the sagittal force vector then remains relatively constant (about 95°) whereas the transverse component swings continually more posteriorly (from 110–130°) until the greatest posterolateral force direction occurs at about two-thirds of stance phase. During the last quarter of stance phase, the longitudinal propulsive component becomes negligible (Fig. 3C) and the sagittal hindlimb force vector swings anteriorly to about 90° (Fig. 4A). At the same time, the transverse forces are dominated by a lateral push on the ground by the hindlimb. This indicates that the last portion of the stance phase (after the time that the fore–aft forces return to zero; Fig. 3C) involves only vertical and lateral forces. Because of the relatively small mediolateral forces, the limb is primarily supporting the body with a secondary role of providing mediolateral stability. The final noisy shifts in hindlimb force orientation just prior to lift-off are inconsequential as they are associated with increasingly trivial force magnitudes.

Integrative dynamics of stance phase for the alligator hindlimb

Our coordinated analyses of hindlimb kinematic, gait, motor pattern, force and bone loading data during stance in alligators (Figs 3, 4) indicate three distinct dynamic phases during this portion of the locomotor cycle for the hindlimb.

Limb-loading phase

During the first fifth of the step, the hindlimb is loaded as body weight is transferred fully to the stance phase forelimb–hindlimb couplet. This limb-loading phase is distinguished by several dynamic features. First, loads on the femur (axial, principal, and shear strains, Fig. 4C–E) increase throughout this phase, rising toward maxima nearly simultaneously by the end of this portion of the step. Gait data (Fig. 3D) show that this phase begins when the hindlimb contacts the substrate and continues until the limbs of the opposing forelimb–hindlimb couplet begin their swing phases

(coincident with the left vertical shaded bar in Figs 3, 4). Joint kinematics (Fig. 3E) show that the knee and ankle both flex as the limb is loaded. However, as the femur is retracted during this phase (continuing motion that began during the previous
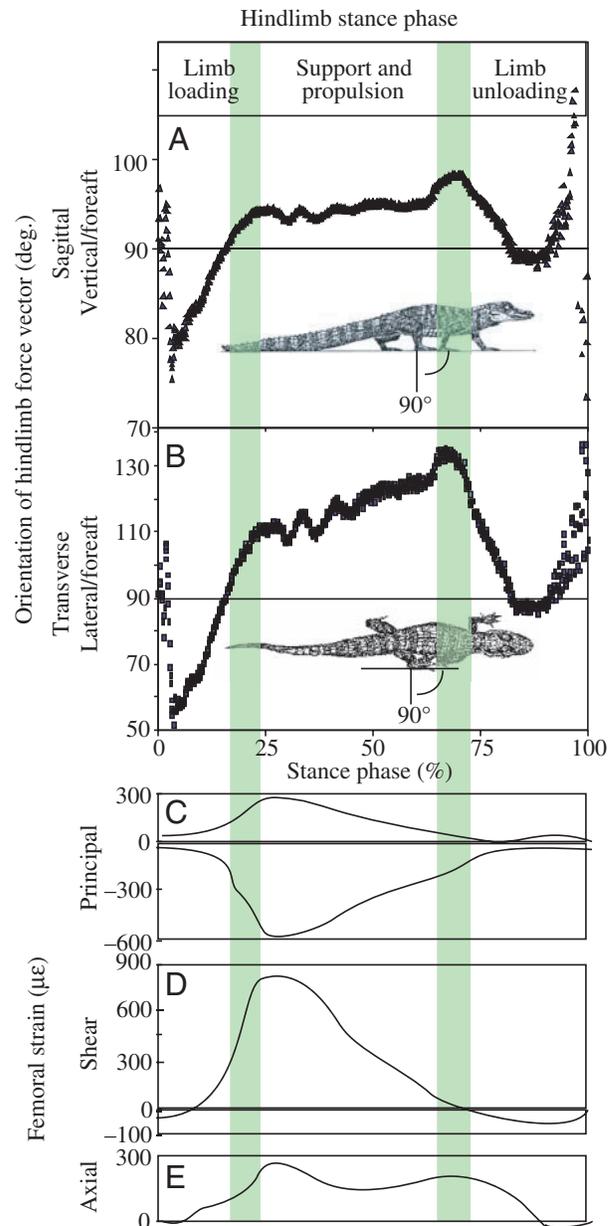

Fig. 4. Typical two-dimensional hindlimb force vectors and femoral strains for alligators using a walking trot. Orientations of the (A) sagittal and (B) transverse hindlimb force vectors are shown in relation to the dynamic hindlimb stance phases shown in Fig. 3 (vertical bars). Note that these vectors are equal in magnitude but opposite in direction to the components of the ground reaction force; thus, when the hindlimb force vector is directed posteriorly (>90°), the ground reaction force is directed anteriorly. (C–E) *In vivo* principal, shear, and axial strains recorded from the alligator femur during the stance phase (at 0.37 m s^{-1}; from Blob and Biewener, 1999). (C,D) Strain traces from the dorsal femur. (E) Strain trace from the anterior femur.

swing phase), femoral adduction remains fairly constant. All of the muscles that will be active during the following propulsive phase have started to contract by the end of the limb-loading phase; in fact, many of these muscles (including CFL, the major limb retractor) start to contract at the end of the swing phase prior to limb loading (Fig. 3F). During the limb loading period, the vertical component of the GRF rises to near maximum levels (>40% body weight), the medial component of the GRF rises to its maximum (10.6% body weight at 19% stance phase), and a small hindlimb braking impulse occurs (Fig. 3C, Table 2). When force components are recalculated to reflect the orientations of forces that the hindlimb exerts on the ground (Fig. 4A,B), sagittally oriented hindlimb forces reflect deceleration during most of the limb-loading phase (i.e. the foot pushing anteriorly on the ground, Fig. 4A), and transversely-oriented hindlimb forces transition from anterolateral at the start of the phase to posterolateral by the end of the phase (Fig. 4B). In addition, the torsional moment of the GRF rises towards its maximum in the lateral direction during the limb-loading phase (clockwise if the right femur is viewed from its proximal end; Fig. 3B), opposite of the direction of rotation that would be expected to result from CFL contraction.

Support-and-propulsion phase

The middle portion of stance phase (between the vertical shaded bars in Figs 3 and 4) is distinguished by several features indicating that hindlimb contributions to body support and propulsion are maximized during this phase. High vertical forces are maintained throughout this phase (Fig. 3C), indicating more or less constant support of body weight by the hindlimb. However, bone strains decrease throughout this phase (Fig. 4C–E) despite the fact that gait diagrams show that the body is supported only by a single limb couplet during this entire phase (Fig. 3D). For the first half of the support and propulsion phase, while the GRF is still increasing (Fig. 3C), decreases in strain probably reflect an increasingly closer alignment between the GRF and the femur. During the second half of the support and propulsion phase, the orientations of the GRF and femur will tend to diverge, but strains continue to decline in correspondence with decreases in GRF magnitude.

Virtually all of the propulsive impulse occurs during this phase (Fig. 3C) with increases to near maximal levels early in this phase. The medially directed GRF decreases from its maximum (of about 6% of body weight) at the onset of this phase to about half maximal values by the end of the support-and-propulsion phase (~64.4% of stance). Ratios of vertical and lateral hindlimb forces to fore-aft hindlimb forces show that the foot exerts a more or less constant but slightly posteriorly directed force on the ground during this phase (Fig. 4A). However, throughout this phase, increases in the rearward force exerted by the foot, and coincident decreases in the lateral force it exerts, result in a 20° posteromedial shift in the direction of the force that the hindfoot exerts on the ground (i.e. transverse forces applied by the hind foot become more

Table 2. *Timing and magnitudes of hindlimb force patterns for high walking alligators*

Variable	Mean ± S.D.
Maximum vertical force	0.532±0.027
Time to maximum vertical force	35.8±2.4
Maximum braking force	0.054±0.018
Time to maximum braking force	6.0±0.7
Time to braking-to-propulsive transition	15.4±0.9
Maximum propulsive force*	–0.059±0.125
Time to maximum propulsive force	64.4±5.4
Maximum lateral force**	–0.106±0.011
Time to maximum lateral force	19.1±1.4

*Negative fore–aft values are accelerative forces.
**Negative mediolateral values are lateral forces.
Forces are in body weight units and times are in percentage of stance duration.
Data are from 20 three-dimensional hindlimb force records pooled across four individuals (N per individual=3, 5, 5, 7) averaging 0.148 m s^{-1} (range 0.110–0.167 m s^{-1}) to match the speed of kinematic and gait data (average 0.146 m s^{-1}) as closely as possible.

posteriorly oriented; Fig. 4B). Limb joint kinematics show that the femur continues to retract during this phase, but that the knee, ankle and femoral adduction angles change little during the first two-thirds of support and propulsion (Fig. 3E). In the last third of the support-and-propulsion phase, femoral retraction continues at the same rate while the knee begins to flex and the ankle begins to extend (plantarflex); thus, shortening of the functional length of the limb caused by knee flexion is counteracted by ankle extension. Consequently, femoral retraction (which stops at the end of this phase) is primarily responsible for overall changes in hindlimb position during the support-and-propulsion phase in alligators. During support-and-propulsion phase, the hip and knee move anteriorly relative to the foot. As a result, when the femur is nearly perpendicular to the body of the alligator (95-100° femoral retraction angle, Fig. 3E), the GRF will shift from being directed anterior to the long axis of the femur (as in the limb-loading phase) to being directed posterior to the long axis of the femur (Blob and Biewener, 2001). As this shift occurs by the midpoint of the support-and-propulsion phase (close to the time of peak vertical force; Fig. 3B), the torsional moment of the GRF about the femur shifts from exerting a lateral moment to a medial moment (counterclockwise when the right femur is viewed from its proximal end; Fig. 3B). This moment reaches its maximum by the end of the support-and-propulsion phase, and it acts to produce femoral rotation in the same direction that is expected from contraction of the CFL. Thus, the actions of both the GRF and CFL have the potential to induce substantial medial rotation of the femur during its retraction in the support-and-propulsion phase. It should be noted, however, that shear strain magnitudes have declined from their maxima by the time during the step that both CFL and the GRF would induce femoral rotation in the same

direction (Fig. 4D). Moreover, CFL activity ceases by the end of this phase (Fig. 3F).

Limb-unloading phase

Dynamic changes in the last third of stance phase delineate the unloading of the hindlimb at the end of the step as the opposite forelimb-hindlimb couplet touchdown and begin their loading phase (Fig. 3D). Limb bone strains decline to zero (Fig. 4C–E) as does propulsive force. The mediolateral component of the GRF decreases to zero during the second half of this phase. Consequently, during the first half of the unloading phase, the sagittal limb forces become more purely vertically oriented as the transverse limb forces become more lateral (Fig. 4A,B). The final, more irregular, portion of the unloading phase reflects rolling over the hindfoot toes. Ratios of vertical and lateral hindlimb forces to fore-aft hindlimb forces decrease from maxima (respectively 130° and 98°, Fig. 4A,B) to minima (~90°) in the first half of this phase, reflecting the decline of all force components to zero toward the end of the step. Most muscles active during the support-and-propulsion phase cease activity very early in the limb unloading phase, with the exception of the knee flexor/ankle extensor gastrocnemius, which is active for nearly the first three quarters of this phase (Fig. 3F). Joint kinematics show that the femur is held in a maximally retracted position during the limb-unloading phase, but that knee flexion and ankle extension continue to counteract each other throughout this phase (Fig. 3E), so that as vertical forces decline the functional length of the limb distal to the knee changes very little in length. The rotational moment about the long axis of the femur also falls to zero by the end of this phase (Fig. 3B).

Discussion

A major motivation for the synthesis of several aspects of alligator limb function in this study was to evaluate how torsional loading of the femur was produced in this species. However, the integration of these datasets also allows us to refine evaluations of how several limb muscles contribute to body weight support and propulsion in alligators, and it provides insights into the terrestrial locomotor mechanics of vertebrates that do not use strictly parasagittal limb posture.

Propulsive forces, in vivo strains, and the hindlimb loading phase

At touchdown, when an alligator first places its hindfoot on the ground, some of its limb joints begin to flex, compressing the functional length of the limb as it begins to support the weight of the body. Although the knee flexes briefly just after foot down, most of the shortening of functional hindlimb length during the limb-loading phase results from ankle flexion. By the end of the limb-loading phase, every stance phase muscle examined was fully active, and the activity of these muscles held the ankle, knee and hip adduction angles nearly constant while the femur is retracted and rotated. Thus, the limb motions that elicit propulsive GRFs by the end of the

limb-loading phase (Figs 3C, 4A,B) relate primarily to femoral retraction and rotation (see also Gatesy, 1991; Blob and Biewener, 2001).

In the alligator femur, principal, shear and longitudinal strains all reach their highest values early in the step by the end of the limb-loading phase or the beginning of the support-and-propulsion phase (Fig. 4C–E). These peak strains coincide with several events, including the point when body weight becomes fully supported by a single limb couplet (Fig. 3D), the onset of the plateau in vertical hindlimb forces (Fig. 3C), the development of peak medial GRFs acting on the hindlimb (Fig. 3C), the end of the hindlimb braking impulse (Fig. 3C), and the peak lateral (outward) rotational moment of the GRF (Fig. 3B). Thus, peak bone loads (i.e., maximum strains) are associated with peak mediolateral forces and moments and the initial loading of body weight onto the limb just prior to the support-and-propulsion phase, rather than with the highest forces associated with propulsion or the support of body weight. Strain magnitudes actually decrease rapidly during the support- and propulsion-phase, even though the body is completely supported by one limb couplet and all hindlimb stance phase muscles are active. Principal and shear strains ultimately return to zero by the end of the support-and-propulsion phase (Fig. 4C,D) as the opposite limb couplet contacts the ground and begins to support body weight (Fig. 3D). Axial strain, however, decreases to zero later during the step than shear strains. This suggests a decline in the importance of torsion relative to bending and axial loads later in the step (perhaps as the leg becomes more closely aligned with the GRF), although this occurs at strain magnitudes much lower than the peak loads experienced earlier in the step.

Mechanisms underlying torsional loading of the alligator femur

Alignment of rotational moments of the GRF with shear strains and muscle activity patterns provides insight into the mechanisms underlying torsional loading of the femur in alligators. Strain records directly indicate the actual deformation of the bone surface, and thus reflect the net loads resulting from all forces acting on the bone. Shear strains (reflecting torsion) increase to their maxima by the end of the limb-loading phase of stance (Fig. 4D) and indicate a medial twisting of the distal end of the femur (Blob and Biewener, 1999). Such twisting could be induced either by the contraction of limb retractor muscles with ventral insertions on the femur, by the rotational moment of the GRF if the GRF is directed posterior to the long axis of the femur or, perhaps, by combined action of both processes. Femoral retractors such as CFL, FTI2 and FTE are active at the end of the limb-loading phase when shear strains are at their highest levels (Fig. 3F), and thus these muscles appear to contribute to the generation of torsional loads on the femur with a tendency to rotate the femur medially. However, when shear strains are highest the GRF is directed *anterior* to the long axis of the femur (Blob and Biewener, 2001) and the GRF exerts a moment that would tend to rotate the femur laterally (Fig. 3B), i.e. in the opposite

direction from rotation induced by the limb retractor muscles. This means that the unusually high shear strains seen in the alligator femur must be produced by contraction of CFL and other muscles *against* the rotational moment of the GRF. This conclusion differs from the hypothesis of Blob and Biewener (2001), who had suggested that high torsional loads in alligator limb bones result because both the GRF and CFL would act additively and induce a moment that would tend to rotate the femur in the same direction. The GRF and CFL do act additively to produce medial femoral rotation later in stance but only after shear strains have begun to decline from their peak. In fact, by the time the GRF exerts its maximum rotational moment in the medial direction at the end of the support-and-propulsion phase (Fig. 3B), activity in the limb retractor muscles ceases (Fig. 3F). Thus, additive action of the GRF and limb retractors (such as CFL) is not a primary factor in the generation of high torsional loads in the alligator femur near the end of the limb-loading phase.

Is femoral torsion a general feature of non-parasagittal locomotion?

The predominance of torsion as a mode of limb bone loading is an unusual feature that distinguishes alligators and iguanas from most tetrapods in which limb bone loads have been evaluated during terrestrial locomotion (Blob and Biewener, 1999). Blob and Biewener (1999) suggested that, if limb bone torsion was a common feature of limb bone loading among crocodilians and lepidosaurs (the broader clades to which alligators and iguanas belong), then it might be a general and, perhaps, ancestral feature of terrestrial locomotor mechanics among species that do not use strictly parasagittal limb movements. However, alligators (and iguanas) exhibit several distinctive kinematic features that are not seen among taxa that habitually use either more or less sprawling limb posture. For example, salamanders, sprawling lizards and mammals all share a distinct pattern of knee kinematics in which flexion is followed by extension during stance phase (Peters and Goslow, 1983; Ashley-Ross, 1995; Reilly, 1995, 2000), whereas alligator and iguana knees are held fixed in early stance and then either extend or flex (Fig. 3; Brinkman, 1980; Reilly and Elias, 1998; Blob and Biewener, 1999). In addition, at the beginning of stance, hip protraction, knee extension, and ankle extension are all greater (by 7–35°, 35–55°, and 30–45°, respectively) in salamanders and sprawling lizards (Ashley-Ross, 1994b; Reilly and Delancey, 1997b; Irschick and Jayne, 1999) than in alligators and iguanas. Thus, whereas alligators and iguanas place the hindfoot under or behind the knee at touchdown, more sprawling taxa (e.g. salamanders and sprawling lizards) use greater limb joint extension at touchdown and are hypothesized to flex these joints to actively pull the body over the foot (Ashley-Ross, 1994b, 1995; Reilly and Delancey, 1997b). Such comparisons of tetrapod kinematics led Ashley-Ross (1994b) to conclude that, in conjunction with femoral retraction, knee flexion and extension are plesiomorphic features of the tetrapod hindlimb cycle.

Alligators differ in that medial rotation of the femur occurs with little change in knee angle.

Generalized tetrapod hindlimb kinematics also appear to be controlled by muscle activity patterns that differ from those used by alligators. For example, the sprawling lizard *Sceloporus clarkii* exhibits distinct EMG patterns in which (1) onset of G activity begins late in swing phase to actively extend the ankle before the foot is placed on the ground, (2) FMTI has a swing phase burst to extend the knee before placing the foot on the ground, and (3) TA has a large burst during early stance that could help to pull the body over the foot (Reilly, 1995). None of these EMG patterns occur in alligators (Fig. 3F).

Even the common muscular function of using the CFL to power hindlimb retraction in alligators and more sprawling taxa (Peters and Goslow, 1983; Reilly, 1995; Gatesy, 1997) could have a different effect on femoral loading because of differences in limb positions used by these animals. In highly sprawling taxa that place the foot far forward at the beginning of stance, the GRF may be directed posterior to the long axis of the femur throughout the duration of stance. If true, then the rotational moment of the GRF and CFL would be in the same direction (both medial). Such an orientation of the GRF might generate low torsional loads (reduced femoral shear strains) among highly sprawling species that initially place the foot far anteriorly, as was found in alligators during the support-and-propulsion phase. Thus, high torsional loads might be a derived feature found among some non-parasagittal taxa including alligators, as opposed to a general feature of non-parasagittal locomotion. Rather than reflecting an ancestral condition, the limb kinematics, muscle activity patterns, and femoral loading patterns of alligators appear to be derived relative to those of other non-parasagittal tetrapods.

Two features of the locomotor apparatus of alligators may result in reductions in overall locomotor effectiveness. First, alligators limit knee flexion-extension and femoral adduction during stance phase. Instead, hindlimb retraction during the support-and-propulsion and limb unloading phases is associated primarily with femoral medial rotation (together with ankle plantarflexion). Consequently, effective vaulting over the stance limbs may be limited. Indeed, walking efficiency is reduced in alligators: although the center of mass rises and falls with each step, little external mechanical energy is recovered by the pendulum-like exchange of kinetic and gravitation potential energies ($19.8\pm2.0\%$; Willey et al., 2004). The second unusual feature of alligator terrestrial locomotion is that the tail is dragged behind the body rather than elevated off of the ground. The long, heavy tail causes the center of mass of alligators to lie more caudally (just in front of the pelvis), so that body weight support is concentrated over the hindlimb (52%) during locomotion (Willey et al., 2004). The constant braking impulse of the tail is countered by propulsive efforts of the limbs. Indeed, in order to balance the braking impulse of the tail, the hindlimb exerts four times the accelerative impulse needed to balance the braking impulse of the forelimb alone (Willey et al., 2004). These necessary modifications in hindlimb function may further limit the ability

of alligators to effectively use vaulting mechanics to recover external mechanical energy

It is noteworthy that iguanas, which also exhibit substantial femoral rotation (and torsion; Blob and Biewener, 1999) also drag large tails behind the body. In contrast, sprawling lizards that lift the tail during locomotion show net propulsive impulses of the hindlimb that balance the net braking impulses of the forelimb (our unpublished data) and much (two to three-fold) greater mechanical efficiency than alligators when walking (Farley and Ko, 1997; S. Reilly, K. Hickey and A. Parchman, unpublished data). With the tail raised, the hindlimbs are only required to counteract the decelerative impulse of the limbs and, thus, lizards may exhibit less axial rotation of the femur and, thereby, lower torsional loads. Experimental verification of these hypotheses remains to be performed. However, the results of our analyses suggest the possibility that patterns of femoral loading in quadrupedal, terrestrial tetrapods may have diversified through evolutionary changes in several lineages, rather than along a single path.

One consequence of the advent of limb rotation in alligators is that several muscles that actively shorten to flex and extend limb joints during stance phase in sprawling (salamanders; Ashley-Ross, 1994b; lizards: Reilly, 1995; Reilly and DeLancey, 1997b) and erect quadrupeds (mammals; Goslow et al., 1973, 1981; Halbertsma, 1983; Smith et al., 1993; Vilensky and Gankiewicz, 1990) must now act in isometric or even eccentric contraction to stabilize the knee and ankle during the support-and-propulsion phase. Although hindlimb EMG data are lacking for iguana, the knee and ankle flexors in alligators are clearly modulated to stiffen the limb during limb rotation. In addition, the same basic leg stiffening pattern is modulated to maintain different fixed joint angles during stance phase across a range of postural heights (Reilly and Blob, 2003). This adds to other recent discoveries (Gillis and Biewener, 2001, 2002, 2003) that counter common assumptions that homologous muscles are used at the same time in the limb cycle across quadrupeds, or to move joints in the same way. In addition, motor patterns in alligator reveal the presence of local and temporal segregation of muscle functions during locomotion. Local segregation is evident in muscles lying side by side (such as the ILTIB1, ILTIB2 and AMB1) that are dedicated to performing different functions in the stance (knee stabilization in the former two) and swing phases (knee extension in AMB1) of the stride. Furthermore, only two (PIT, ILTIB1) of our 16 muscles had clear functions in both stance and swing phases. Most notably, PIT appears to aid other muscles (ADD1, PIFE3) in supporting the body weight during the stance phase, while it is alone in counteracting femoral abduction (by the ILFIB, ILFEM) during swing phase. These results point to several future directions for research on iguanas, sprawling lizards and semi-erect mammals that could improve understanding of the effects of posture, tail dragging, and phylogeny on the diversity of quadrupedal locomotor mechanisms.

References

Alexander, R. McN. (1974). The mechanics of a dog jumping, *Canis familiaris*. *J. Zool. Lond.* **173**, 549-573.

Alexander, R. McN. and Jayes, A. S. (1983). A dynamic similarity hypothesis for the gaits of quadrupedal mammals. *J. Zool. Lond.* **201**, 135-152.

Ashley-Ross, M. A. (1994a). Metamorphic and speed effects on hindlimb kinematics during terrestrial locomotion in the salamander *Dicamptodon tenebrosus*. *J. Exp. Biol.* **193**, 285-305.

Ashley-Ross, M. A. (1994b) Hindlimb kinematics during terrestrial locomotion in a salamander (*Dicamptodon tenebrosus*). *J. Exp. Biol.* **193**, 255-283.

Ashley-Ross, M. A. (1995). Patterns of hindlimb motor output during walking in the salamander *Dicamptodon tenebrosus*, with comparisons to other tetrapods. *J. Comp. Physiol. A.* **177**, 273-285.

Bakker, R. T. (1971). Dinosaur physiology and the origin of mammals. *Evolution* **25**, 636-658.

Biewener, A. A. (1989). Scaling body support in mammals: limb posture and muscle mechanics. *Science* **245**, 45-48.

Biewener, A. A. (1990). Biomechanics of mammalian terrestrial locomotion. *Science* **250**, 1097-1103.

Biewener, A. A. (1992). *In vivo* measurement of bone strain and tendon force. In, Biomechanics – Structures and Systems: A Practical Approach (ed. A.A. Biewener), pp. 123-147. New York: Oxford University Press.

Biewener, A. A. and Dial, K. P. (1995). *In vivo* strain in the humerus of pigeons (*Columba livia*) during flight. *J. Morphol.* **225**, 61-75.

Biewener, A. A., Thomason, J., Goodship, A. and Lanyon, L. E. (1983). Bone stress in the horse forelimb during locomotion at different gaits: a comparison of two experimental methods. *J. Biomech.* **16**, 656-576.

Biewener, A. A., Thomason, J. and Lanyon, L. E. (1988). Mechanics of locomotion and jumping in the horse (*Equus*): *in vivo* stress in the tibia and metatarsus. *J. Zool. Lond.* **214**, 547-565.

Blickhan, R. and Full, R. J. (1992). Mechanical work in terrestrial locomotion. In *Biomechanics: Structures and Systems* (ed. A. A. Biewener), pp. 75-96. New York: Oxford University Press.

Blob, R. W. (2001). Evolution of hindlimb posture in nonmammalian therapsids: biomechanical tests of paleontological hypotheses. *Paleobiol.* **27**, 14-38.

Blob, R. W. and Biewener, A. A. (1999). *In vivo* locomotor strain in the hindlimb of *Alligator mississippiensis* and *Iguana iguana*: implications for the evolution of limb bone safety factor and non-sprawling limb posture. *J. Exp. Biol.* **202**, 1023-1046.

Blob, R. W. and Biewener, A. A. (2001). Mechanics of limb bone loading during terrestrial locomotion in the green iguana (*Iguana iguana*) and American alligator (*Alligator mississippiensis*). *J. Exp. Biol.* **204**, 1099-1122.

Brinkman, D. (1980). The hindlimb step cycle of *Caiman sclerops* and the mechanics of the crocodile tarsus and metatarsus. *Can. J. Zool.* **58**, 2187-2200.

Carrano, M. T. (1998). Locomotion in non-avian dinosaurs: integrating data from hindlimb kinematics, *in vivo* strains and bone morphology. *Paleobiol.* **24**, 450-469.

Cavagna, G. A., Heglund, N. C. and Taylor, C. R. (1977). Mechanical work in terrestrial locomotion: two basic mechanisms for minimizing energy expenditure. *Am. J. Physiol.* **233**, R243-R261.

Charig, A. J. (1972). The evolution of the archosaur pelvis and hindlimb: an explanation in functional terms. In *Studies in Vertebrate Evolution* (ed. K. A. Joysey and T. S. Kemp), pp. 121-155. Edinburgh: Oliver and Boyd.

Daley, J. W. and Riley, W. F. (1978). *Experimental Strain Analysis* New York: McGraw-Hill.

Demes, B., Larson, S., Stern, J. T., Jr, Jungers, W. L., Biknevicius, A. R. and Schmitt, D. (1994). The kinetics of primate quadrupedalism: "hind limb drive" reconsidered. *J. Human Evol.* **26**, 353-374.

Farley, C. T. and Ko, T. C. (1997). Mechanics of locomotion in lizards. *J. Exp. Biol.* **200**, 2177-2188.

Gatesy, S. M. (1990). Caudofemoralis musculature and the evolution of theropod locomotion. *Paleobiol.* **16**, 170-186.

Gatesy, S. M. (1991). Hindlimb movements of the American alligator (*Alligator mississippiensis*) and postural grades. *J. Zool.* **224**, 577-588.

Gatesy, S. M. (1997). An electromyographical analysis of hindlimb function in *Alligator* during terrestrial locomotion. *J. Morphol.* **234**, 197-212.

Gillis, G. B. and Biewener, A. A. (2001). Hindlimb muscle function in relation to speed and gait: in vivo patterns of strain and activation in a hip and knee extensor of the rat (*Rattus norvegicus*). *J. Exp. Biol.* **204**, 2717-2731.

Gillis, G. B. and Biewener, A. A. (2002). Effects of surface grade on proximal hindlimb muscle strain and activation during rat locomotion. *J. Appl. Physiol.* **93**, 1731-1743.

Gillis, G. B. and Biewener, A. A. (2003). The importance of functional plasticity in the design and control of the vertebrate musculoskeletal system. In *Vertebrate Biomechanics and Evolution* (ed. V. L. Bels, J. P. Gasc and A. Casinos). Oxford, UK: Bios Scientific Publishers.

Goslow, G. E., Jr, Reinking, R. M. and Stuart, D. G. (1973). The cat step cycle: hindlimb joint angles and muscle lengths during unrestrained locomotion. *J. Morph.* **141**, 1-42.

Goslow, G. E., Jr, Seeherman, H. J., Taylor, C. R., McCutchin, M. N. and Heglund, N. C. (1981). Electrical activity and relative length changes of dog limb muscles as a function of speed and gait. *J. Exp. Biol.* **94**, 15-42.

Halbertsma, J. M. (1983). The stride cycle of the cat: the modeling of locomotion by computerized analysis of automatic recordings. *Acta Physiol. Scand.* (Suppl.) **521**, 1-75.

Hildebrand, M. (1976). Analysis of tetrapod gaits: general considerations and symmetrical gaits. In *Neural Control of Locomotion* Vol. 18. (ed. R. M. Herman, S. Grillner, P. Stein and D. G. Stuart), pp. 203-206. Plenum. New York.

Irschick, D. J. and Jayne, B. C. (1999). Comparative three-dimensional kinematics of the hindlimb for high-speed bipedal and quadrupedal locomotion of lizards. *J. Exp. Biol.* **202**, 1047-1065.

Jayne, B. C., Reilly, S. M., Wainwright, P. C. and Lauder, G. V. (1990). The effect of sampling rate on the analysis of digital electromyograms from vertebrate muscle. *J. Exp. Biol.* **154**, 557-565.

Jenkins, F. A. Jr (1971). Limb posture and locomotion in the Virginia opossum (*Didelphis virginiana*) and in other non-cursorial mammals. *J. Zool.* **165**, 303-315.

Parchman, A. J., Reilly, S. M. and Biknevicius, A. R. (2003). Whole-body mechanics and gaits in the gray short-tailed opossum, *Monodelphis*

domestica: kinetic and kinematic patterns of locomotion in a semi-erect mammal. *J. Exp. Biol.* **206**, 1379-1388.

Peters, S. E. and Goslow, G. E. J. (1983). From salamanders to mammals: continuity in musculoskeletal function during locomotion. *Brain Behav. Evol.* **22**, 191-197.

Parrish, J. M. (1986). Locomotor adaptations in the hindlimb and pelvis of the thecodontia. *Hunteria* **1**, 1-35.

Parrish, J. M. (1987). The origin of crocodilian locomotion. *Paleobiol.* **13**, 396-414.

Pennycuick, C. J. (1967). The strength of the pigeon's wing bones in relation to their function. *J. Exp. Biol.* **46**, 219-233.

Pridmore, P. A. (1985). Terrestrial locomotion in monotremes (Mammalia: Monotremata). *J. Zool.* **205A**, 53-73.

Reilly, S. M. (1995). Quantitative electromyography and muscle function of the hindlimb during locomotion in the lizard *Sceloporus clarkii. Zoology: Anal. Compl. Syst.* **98**, 263-277.

Reilly, S. M. (2000). Locomotion in the quail (*Coturnix japonica*): the kinematics of walking and increasing speed. *J. Morphol.* **243**, 173-185.

Reilly, S. M. and Biknevicius, A. R. (2003). Integrating kinetic and kinematic approaches to the analysis of terrestrial locomotion. In *Vertebrate Biomechanics and Evolution* (ed. V. L. Bels, J. P. Gasc and A. Casinas), pp. 243-265. Oxford, UK: BIOS Scientific Publishers.

Reilly, S. M. and Blob, R. W. (2003). Motor control of locomotor hindlimb posture in the American alligator (*Alligator mississippiensis*). *J. Exp. Biol.* **206**, 4341-4351.

Reilly, S. M. and DeLancey, M. J. (1997a). Sprawling locomotion in the lizard *Sceloporus clarkii*: the effects of speed on gait, hindlimb kinematics, and axial bending during walking. *J. Zool.* **243**, 417-433.

Reilly, S. M. and DeLancey, M. J. (1997b). Sprawling locomotion in the lizard *Sceloporus clarki*: quantitative kinematics of a walking trot. *J. Exp. Biol.* **200**, 753-765.

Reilly, S. M. and Elias, J. A. (1998). Locomotion in *Alligator mississippiensis*: kinematic effects of speed and posture and their relevance to the sprawling to erect paradigm. *J. Exp. Biol.* **201**, 2559-2574.

Rewcastle, S. C. (1981). Stance and gait in tetrapods: an evolutionary scenario. *Symp. Zool. Soc. Lond.* **48**, 239-267.

Romer, A. S. (1923). Crocodilian pelvic muscles and their avian and reptilian homologues. *Bull. Am. Mus. Nat. Hist.* **48**, 533-552.

Rubin, C. T. and Lanyon, L. E. (1982). Limb mechanics as a function of speed and gait: a study of functional strains in the radius and tibia of horse and dog. *J. Exp. Biol.* **101**, 187-211.

Smith, J. L., Chung, S. H., and Zernicke, R. F. (1993). Gait-related motor patterns and hindlimb kinematics for the cat trot and gallop. *Exp. Brain Res.* **94**, 308-322.

Snyder, R. C. (1962). Adaptations for bipedal locomotion in lizards. *Am. Zool.* **2**, 191-203.

Swartz, S. M., Bennett, M. B. and Carrier, D. R. (1992). Wing bone stresses in free flying bats and the evolution of skeletal design for flight. *Nature* **359**, 726-729.

Updegraff, G. (1990). *Measurement TV: Video Analysis Software.* San Clemente, CA: Data Crunch.

Vilensky, J. A. and Gankiewicz, E. (1990). Effects of growth and speed on hindlimb joint angular displacement patterns in vervet monkeys (*Cercopithecus aethiops*). *Am. J. Phys. Anthropol.* **81**, 441-449.

Willey, J. S., Biknevicius, A. R., Reilly, S. M. and Earls, K. D. (2004). The tale of the tail: limb function and locomotor mechanics in *Alligator mississippiensis. J. Exp. Biol.* **207**, 553-563.